Aircraft fuselage effects on transonic wing pressures via Non-Linear Vortex Lattice Method

Vincent Liguori, Frederic Moens, Jacques Peter, Eric Laurendeau

Association Aéronautique et Astronautique de France

57th 3AF International Conference on Applied Aerodynamics
29 — 31 March 2023, Bordeaux – France

AERO2023-81-LIGUORI

Aircraft fuselage effects on transonic wing pressures via Non-Linear Vortex Lattice Method

Vincent Liguori[(1)], Frederic Moens[(2)], Jacques Peter[(3)], Eric Laurendeau[(4)]
[(1)]*ONERA, 8 rue des Vertugadins, Meudon, France, vincent.liguori@onera.fr*
[(2)]*ONERA, 8 rue des Vertugadins, Meudon, France, frederic.moens@onera.fr*
[(3)]*ONERA, 29 Av. de la Division Leclerc, Chatillon France, jacques.peter@onera.fr*
[(4)]*Polytechnique Montréal, 2500 Chem. de Polytechnique, Montréal, Quebec, Canada, eric.laurendeau@polymtl.ca*

ABSTRACT

The implementation of the Non-Linear Vortex Lattice Method in the CHAMPS framework is presented. Developments are made with the aim of improving the prediction of pressure distributions in the region near the root of the wing with physics-based modifications. The viscous coupling algorithm is modified to better take into account compressibility effects on swept wings. A methodology to better capture the spanwise variation of the flow caused by the wing-body geometry while computing the database used for the viscous coupling is tested. Results for the isolated modifications are shown. The results of the complete methodology applied on classical test cases of the DLR F4 wing-body and the High-Speed Common Research Model wing-body are shown. Improvements in shock prediction are observed however limitations associated to drag overprediction are identified.

1. INTRODUCTION

Potential methods based on a distribution of discrete perturbations to represent the geometry of a body are useful tools in the context of early aircraft design phases because of their low computational cost compared with other higher fidelity methods such as Reynolds-Averaged Navier-Stokes (RANS) equations solver [16]. They can in particular model adequately the spanwise distribution of the induced angle of attack on a wing caused by a lift distribution. These methods in their original forms are limited by their underlying assumptions of inviscid, incompressible and irrotational flow.

These limitations can be partially overcome by adding corrections to the original potential equations to take into account the phenomena that would otherwise be neglected. Many such approaches have been tested in the literature. Notably, to consider some compressibility effects up to the transonic regime the Prandtl-Glauert transformation can be used. To consider additional phenomena such as viscosity and shocks, coupling the potential method with higher fidelity data is a popular method that has been applied by numerous authors with various methodologies, as compiled in the literature [20].

The work presented in this paper uses a methodology of this type, based on coupling a Vortex Lattice Method (VLM) with two-dimensional viscous data computed from a RANS solver to correct the local lift and drag coefficients using strip-theory. This method is referred to as Non-Linear Vortex Lattice Method (NL-VLM) and is implemented in the CHAMPS framework developed at École Polytechnique de Montréal [13][11].

While the method has demonstrated a good agreement with higher fidelity solvers and experimental data in low-speed and transonic conditions, the prediction of shocks in transonic conditions near the fuselage in the root region of the wing has been identified as a limitation of the method. In one previous work [4], the method was seen predicting shocks in this region when a gradual pressure decrease was observed experimentally. In another previous work [8], the method predicted the appearance of large shocks that caused stalling of the wing sections near the fuselage in transonic conditions, which did not match with numerical results computed using a more computationally intensive 3D RANS method.

Based on this observation, modifications to the implementation of NL-VLM were tested in this paper with the

goal of improving the prediction of shocks on wing-body configurations in the wing region near the fuselage in transonic flow conditions.

The numerical implementation of the NL-VLM algorithm without the modifications is first summarized. A more detailed description of the modifications to the methodology compared with previous implementations is then presented. Numerical results obtained on the wing-body configurations of the DLR-F4 and Common Research Model geometries in transonic conditions are finally shown. The effects of the modifications on these test cases are then discussed.

2. INITIAL NON-LINEAR VORTEX LATTICE METHOD IMPLEMENTATION

The NL-VLM implementation is based on a potential three-dimensional method, a two-dimensional higher fidelity method to create a viscous database, a coupling algorithm to correct the potential method with the viscous database and a methodology to compute the total forces over the body from the coupled system. The initial implementation of these main steps is presented in this section. The NL-VLM in the CHAMPS framework is already described in the literature [11], as such unchanged parts of the methodology are briefly summarized to the extent required for the subsequent description of the modifications applied in the context of this work in Sec. 3.

2.1 Three dimensional potential method

To model the three-dimensional geometry, a potential method with hybrid elements is used. The geometry is considered to be an assembly of two categories of bodies. The first category is made of lifting surfaces, which are considered to be thin bodies. In the case of this work, this category is used for wing surfaces. These bodies are modeled using a classical vortex-lattice method [6]. A structured grid is placed over the planform of the wing, simplified as being flat between the leading edge and trailing edge. Vortex ring elements are then placed at the quarter length of the structured grid elements.

The second type of bodies are non-lifting bodies, which are considered to be bluff bodies. In the case of this work, this category is used for fuselages. These bodies are modeled using an unstructured constant source panels method, the panels being placed over the surface of the bodies.

For both types of elements, a Neumann boundary condition of velocity tangent to the element is imposed. This condition is verified at a control point placed at the center of the element in the case of the source panels and at 3/4 of the length of the elements for the vortex rings, which allows the vortex rings to create lift with a slope corresponding to thin airfoil theory [1][15]. The complete system considering both vortex ring and source panel elements is solved to compute the intensity of the perturbations. To improve the accuracy of the model in transonic conditions, the Prandtl-Glauert transformation is applied to both types of elements [2].

2.2 Viscous database

The viscous database consists of tables of lift, drag and moment coefficients of an airfoil for a range of angles of attack. These coefficients are obtained with the CHAMPS RANS equations solver, which is a solver using a cell-centered finite-volume approach. A more detailed description of the solver and its capabilities is outside the scope of this work but is available in the literature [13]. These tables of coefficients are computed for airfoils representing chosen sections along the span of the wing. The database is then interpolated along the wing span so that a corresponding local viscous database is allocated to every wing strip.

Since wing sweep has an important effect on flow fields around airfoils, it has been shown that simply using a 2D RANS simulation is insufficient to obtain solutions that match experimental results both in force coefficients and pressure distribution [4]. Wing sweep effects are considered in the viscous database calculation through a 2.5D approach to consider an infinitely swept wing of constant geometry instead of a straight wing. This is done using a "sheared-mesh" approach in which a 2D mesh is extruded in a third dimension over 1 cell. The extrusion direction is aligned with the quarter-chord sweep angle of the wing. A periodic boundary condition is then applied on the side faces of the mesh created during the extrusion. An alternative is to directly implement the 2.5D hypothesis in the RANS equations, removing the need for halo-cells [5]. The former method can be viewed as a discrete form, the latter as a continuous form. In this paper, the discrete form is used.

2.3 Viscous Coupling

The method uses a coupling between the inviscid method and a viscous database to include non-linear effects. This coupling is done only on lifting elements by forcing the chordwise sections of the wing in the potential flow to match the lift of their corresponding viscous database at their effective angle of attack. To enforce this, the algorithm used is inspired by Van Dam's α-coupling method [17], which consists in rotating the normal vector of the elements by a viscous coupling correction angle to influence the vortex intensity of the elements. The coupling methodology, similar to the loosely coupled algo-

rithm used by Gallay and Laurendeau [4], is summarized as

1. Compute the sectional lift coefficient of the local strip in the inviscid potential flow using the Kutta-Joukowski theorem [6]
2. Compute the local effective angle of attack α_e from the theoretical lift slope of the wing section.
3. Obtain through interpolation the lift coefficient at the computed effective angle of attack from the viscous database.
4. Update a viscous coupling correction angle based on the difference between the two lift coefficients.
5. Apply a rotation to the normal of the elements in the section corresponding to the viscous coupling correction angle.

These steps are repeated iteratively for each chordwise strip of elements until the difference between the viscous and inviscid lift coefficients is sufficiently small, at which point the update to the viscous correction angle will tend toward zero and convergence is considered achieved.

2.4 Force Coefficients Computation

The lift and moment coefficients are computed from the potential solution using the Kutta-Joukowski theorem. The drag coefficient is computed in two parts. The induced drag is computed using a Trefftz plane [6] and the viscous and pressure components of the drag are computed by integrating the corresponding drag coefficients at the effective angle of attack of the viscous database for each wing section. Both contributions are summed to obtain the total drag. A more detailed description of the methodology is available in a previous presentation of the method [11].

3. MODIFICATIONS TO THE NL-VLM IMPLEMENTATION

The three modifications applied to the NL-VLM are the use of a new equation to compute the local effective angle of attack, taking into account the taper of the wing in the viscous database computation and adding a new boundary condition in the computation of the viscous database to model the perturbation effect of the fuselage.

3.1 Calculation of the local effective angle of attack

The coupling algorithm presented in section 2.3 computes the local effective angle of attack by dividing the inviscid lift coefficient of the section by a theoretical local lift slope value.

The collocation points in the VLM method are placed to ensure a local slope of 2π in the case of an infinite unswept wing with no other transformation being applied in accordance with the 1/4-3/4 rule of Pistolesi [15]. The Prandtl-Glauert correction and the presence of sweep however have an influence on the lift slope of the elements.

In a previous work [14] these effects are considered with two distinct multiplying factors, so that

$$C_{L\alpha,inv} = \frac{2\pi cos(\Phi)}{(\beta)} \tag{1}$$

$$\beta = \sqrt{1-M^2} \tag{2}$$

where Φ is the sweep angle of the quarter-chord of the wing, β is the Prandtl-Glauert transformation factor and M is the Mach number of the freestream. In another previous work the lift slope used is taken for each section directly from the linear part of the lift slope in the viscous database [7]. In this work, the lift slope used is the theoretical lift slope of an infinite swept wing in a potential field where the Prandtl-Glauert transformation has been applied, derived in the literature [2] as

$$C_{L\alpha,inv} = \frac{2\pi cos(\Phi)}{\sqrt{\beta^2 \cos^2(\Phi) + \sin^2(\Phi)}}. \tag{3}$$

In the two limiting cases of an unswept wing and a Mach number of zero, Eq. 1 and Eq. 3 are equivalent. They however differ when both effects are present simultaneously. To validate this approach, the VLM code without viscous coupling is used on the case of a swept wing with an aspect ratio of 1000, which is close to an infinite wing. The sweep angle used is 26.57 degrees and the Mach number used for the Prandlt-Glauert transformation is 0.85.

It can be seen in Fig. 1 that the new theoretical lift slope is closer to the numerical results than the previous method. Using the approach of estimating the effective angle of attack by assuming that the local lift slope corresponds to the infinite swept wing case with the local section geometry, the new method is considered more accurate than the previous formula to compute the effective angle of attack. In contrast with the method of using the linear section of the viscous slope shown in the literature, this method is only based on inviscid flow and as such is considered more representative of the numerical method. It also does not require the delicate step of identifying the linear part of the viscous slope for every wing section.

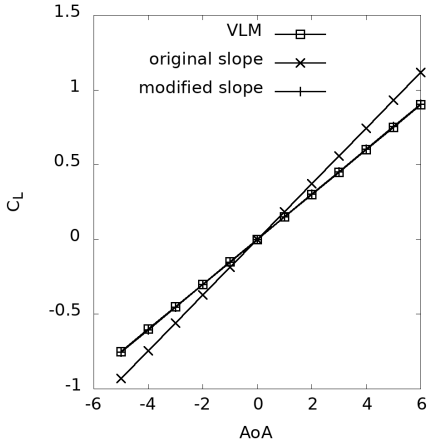

Figure 1: Comparison of the initial and modified lift slope with the numerical results of the VLM on an near-infinite swept wing (Ma=0.85, ϕ=26.57°)

3.2 Consideration of tapered geometry in viscous database

As mentioned in Sec. 2.2, a 2.5D sheared-cell approach is used in the initial method. This deformation of the mesh only considered the quarter-chord sweep of the wing section. However, the difference in sweep between the leading edge and the trailing edge in a tapered wing could lead to differences in flow solutions, particularly near the stall angle.

The region of the wing near the fuselage is usually more tapered than the outboard sections of the wing for transonic transport aicraft, this difference being visually identifiable at a kink in the wing trailing edge. For this reason, a new mesh deformation method was tested to model the taper effect during the viscous database computation for sections in this region. This new method consists in varying the extrusion direction of the 2D mesh based on the location relative to the airfoil.

The mesh points located upstream of the leading edge of the airfoil are moved in the direction of the leading edge sweep. The extrusion direction of the mesh points located between the leading edge and trailing edge varies linearly between the leading edge sweep and trailing edge sweep so that the taper ratio is applied to the extruded mesh. Finally, the points located downstream of the trailing edge are moved in the direction of the trailing edge sweep. To keep the airfoil section consistent, a vertical scaling corresponding to the taper ratio is also applied to the mesh points located between the lowest and highest points of the airfoil. A schematic representation of this extrusion method from a top-view can be seen in Fig. 2. The airfoil is shown with continuous lines and the mesh extrusion direction is shown in dashed lines. Using this methodology, the taper effects are considered directly by the physics of the solver similarly to recent 2.5D approaches [5][3], in contrast with other approaches for taper effects in the literature based on subsequent correction of non-tapered results [19].

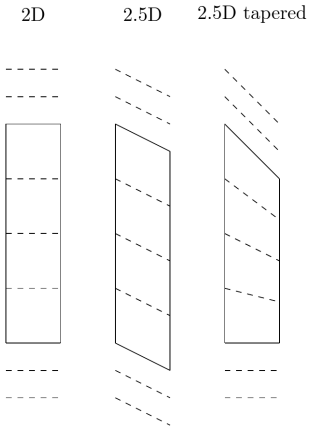

Figure 2: Schematic top view of the extruded mesh with 2D, 2.5D and 2.5D tapered geometries

This varying deformation has the effect of creating a difference between the geometries at the end of the extrusion. In the limiting case of a large enough extrusion, mesh cells in the airfoil region would eventually cross and create negative volumes. Even before this limiting case, a large variation of chord could have a non-negligible impact on the average Reynolds number of the flow over the airfoil. To avoid these effects, a parametric study is done on the extrusion length of the airfoil and its impact on the obtained aerodynamic coefficients. The results, shown in Fig. 3, indicate that the results tend to converge when a sufficiently small extrusion length is used. Based on these results the extrusion length used in this work for a tapered geometry is fixed at five percent of the chord.

To validate the hypothesis that this modification allowed the solver to capture physical phenomena caused by the tapered geometry, a comparison is made between the surface solution obtained with the tapered extrusion and the original 2.5D method. The test case corresponds to the airfoil at the wing root of the High-Speed Common Research Model (HS-CRM) geometry [18], used notably in the fifth AIAA drag prediction workshop [10]. The flow conditions are those of the first test case of the workshop, namely a Mach number of 0.85 and a global Reynolds number of 5 000 000 which corresponds to a Reynolds number of 8 461 600 relative to the local chord since the global Reynolds number uses the mean aerodynamic chord as a reference length.

A top-view of the wall shear stress lines in Fig. 4 and Fig. 5 before stall for each configuration reveals that there is higher convection by a crossflow in the 2.5D case compared with the 2.5D tapered case near the trailing edge

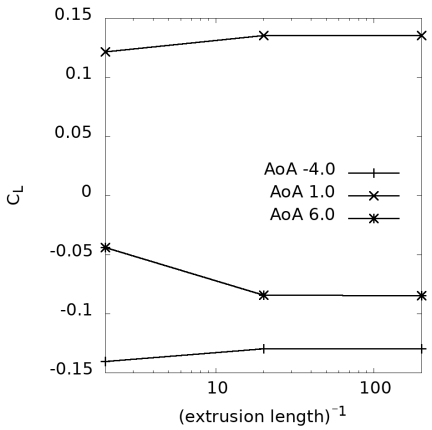

Figure 3: Lift coefficient for various angle of attacks using tapered extrusion method relative to the inverse of the extrusion length (Ma=0.85, Re=8.46e6, ϕ_{LE}=37.1°, ϕ_{TE}=9.8°)

of the airfoil. This behavior is expected and shows that the method is able to capture the difference caused by the geometry. A comparison of the lift coefficients in Fig. 6 shows the impact of this difference on the stall behavior. Notably, a steeper loss of lift is observed in the 2.5D tapered case after the onset of stall. It is also noted during testing that this mesh modification significantly hampers the convergence of the solver. In some instances, stabilization techniques such as Selective Frequency Damping [12] are used to obtain converged solutions.

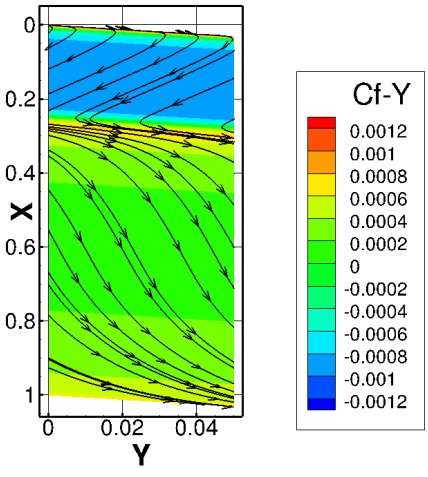

Figure 4: Wall shear stress lines and y-direction shear stress contour for the 2.5D case at an angle of attack of 1.0 (Ma=0.85, Re=8.46e6, ϕ_{LE}=37.1°, ϕ_{TE}=9.8°)

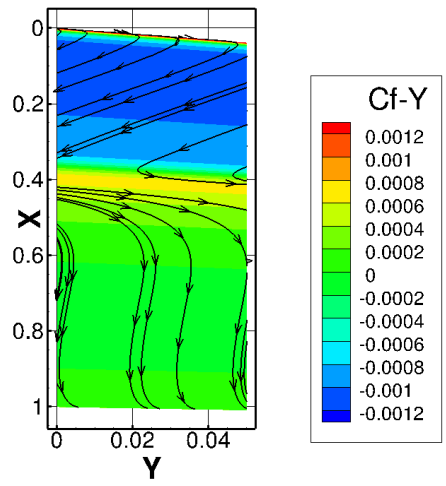

Figure 5: Wall shear stress lines and y-direction shear stress contour for the 2.5D tapered case at an angle of attack of 1.0 (Ma=0.85, Re=8.46e6, ϕ_{LE}=37.1°, ϕ_{TE}=9.8°)

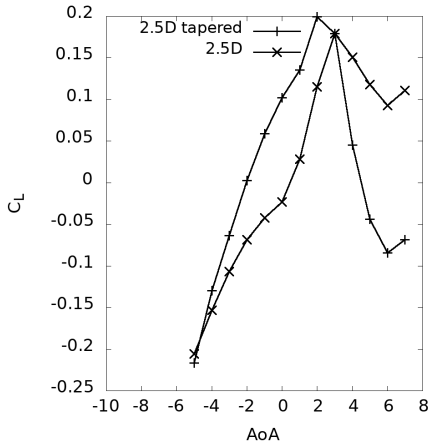

Figure 6: Lift coefficient curves comparison between the 2.5D geometry and the 2.5D tapered geometry (Ma=0.85, Re=8.46e6, ϕ_{LE}=37.1°, ϕ_{TE}=9.8°)

3.3 Consideration of fuselage effect on crossflow in viscous database

The last modification aims to model the fact that, near the root of the wing, the presence of the fuselage reduces the crossflow over the wing. In the initial implementation, this variation in crossflow is not considered in the computation of the viscous database since the 2.5D approach assumes an infinite swept wing and as such no spanwise variation of crossflow.

To model this variation of crossflow, the boundary conditions applied on the extruded 2.5D mesh are modified. Instead of a periodic boundary condition on the faces of the mesh in the extrusion direction, a symmetry condition is applied on the face at the inboard side of the extruded

airfoil. A zero-order extrapolation boundary condition is applied to the outboard side face so that the values of each conservative variable are copied in their corresponding halo cell. This approach creates a spanwise variation in the crossflow between the two extrusion faces of the mesh.

This approach is tested on a near-root airfoil section of the DLR-F4 wing body. This geometry was used in the first drag prediction workshop [9] and has also already been tested in a previous work with a NL-VLM approach using a RANS 2.5D database [4]. The flow conditions correspond to the first test case of the workshop, which are a lift coefficient of 0.5, a Reynolds number of 3 000 000 using the mean aerodynamic chord as the reference length and a Mach number of 0.75. In this previous work the shock prediction in the section with pressure measurement nearest to the fuselage did not match the experimental results.

The test case is first solved with the initial NL-VLM implementation to obtain a spanwise lift distribution. Four 2.5D polars are used to create the original viscous database, using the root section, the kink section with two different sweeps corresponding to the wing sweep before and after the kink and the wing tip section. The airfoil section at 18.5% of the span away from the symmetry plane is then extracted and the local lift coefficient obtained through the initial NL-VLM solver is used as a reference for the section. This section is selected because it is the nearest section to the fuselage for which pressure measurements were taken in experimental testing.

The section is then tested with the CHAMPS RANS solver in its local flow conditions using the original 2.5D approach and the modified boundary condition approach, each time matching the same section lift coefficient. In both cases, an extrusion distance of 1 chord is used. The goal of this test is to investigate if the modification of the boundary condition improves the agreement between the pressure coefficients of the RANS solver and the experimental result. The pressure coefficients distribution obtained in Fig. 7 shows that the modified boundary conditions approach predicts a distribution closer to the experimental results. In particular, the shock over the upper surface predicted in the original 2.5D approach is not present with the new approach.

Since the new boundary conditions create a variation in crossflow between the two extrusion faces of the mesh, it is expected that varying the extrusion length would have an impact on the result. This is confirmed in Fig. 8 and Fig. 9, showing a parametric study of the extrusion length when using the one-sided symmetry approach. This parametric study is on the same HS-CRM root airfoil test case shown in Sec. 3.2. The same results with the original 2.5D approach are also shown for comparison. The aero-

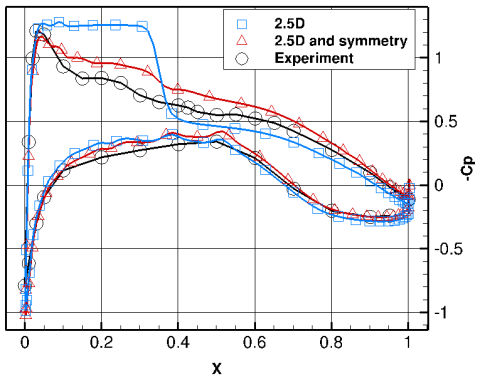

Figure 7: Pressure coefficients comparison of the 2.5D and 2.5D with symmetry condition approach at equivalent lift with experimental results (Ma=0.75, Re=3.92e6, $\phi_{c/4}$=21.0°)

dynamic coefficients tend toward the 2.5D results when the extrusion length becomes large. This is expected and reflects the fact that since the extrusion is done over only one cell in which the solver assumes a linear variation and that one face imposes a null crossflow, increasing the distance between the two faces reduces the spanwise component of the crossflow gradient since the variation is performed over a larger distance. In the limiting case of an infinite-length extrusion, the results would converge toward the original 2.5D case. When applying the one-sided symmetry methodology, two behaviors are observed. The first one is an increase in C_{Lmax} and of the stall angle of attack. The second one is a global increase in drag.

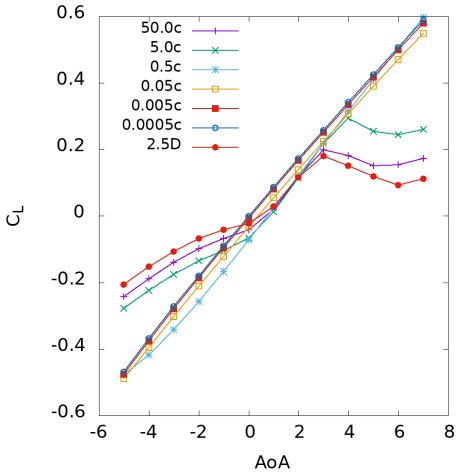

Figure 8: Parametric study of extrusion length when using a symmetry condition at root for lift coefficient against angle of attack and comparison with 2.5D approach (Ma=0.85, Re=8.46e6, $\phi_{c/4}$=31.4°)

The extrusion length impact is problematic for two rea-

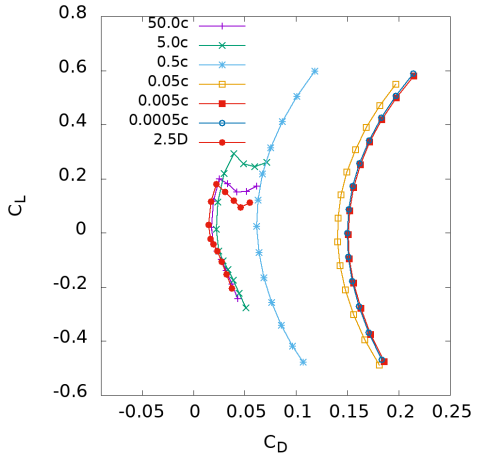

Figure 9: Parametric study of extrusion length when using a symmetry condition at root for lift coefficient against drag coefficient and comparison with 2.5D approach (Ma=0.85, Re=8.46e6, $\phi_{c/4}$=31.4°)

sons. The first one is that it was observed in the tapered geometry database investigation in Sec. 3.2 that the extrusion length has an impact on the results and that a small extrusion length relative to the chord is desirable. The second reason is practicality, since modifying a mesh is a more time-demanding procedure compared to varying a numerical coefficient, particularly if multiple values must be tested for a parametric study. To avoid these difficulties, a new boundary condition is implemented in the RANS solver. For this boundary condition, the density and pressure of the interior cell are copied in the halo cell, while the velocity is set so that a predetermined percentage of the normal velocity through the face of the boundary is canceled. The implementation is summarized as:

$$\begin{aligned} \rho_{halo} &= \rho_{in} \\ p_{halo} &= p_{in} \\ v_{x,halo} &= v_{x,in} - 2k(\vec{v}_{in}\cdot\vec{n})\cdot n_x \\ v_{y,halo} &= v_{y,in} - 2k(\vec{v}_{in}\cdot\vec{n})\cdot n_y \\ v_{z,halo} &= v_{z,in} - 2k(\vec{v}_{in}\cdot\vec{n})\cdot n_z \end{aligned} \tag{4}$$

where ρ is the density, p is the pressure, $\vec{v}$ is the velocity at the cell center and $\vec{n}$ is the unit normal vector for the boundary face. The halo cell and the interior cell are identified with their respective indices and the x,y and z indices identify the directional components of vectors. The parameter k is the normal forcing factor and is set by the user. In the limiting case where $k = 1.0$, the boundary condition is equivalent to a symmetry condition. In the limiting case where $k = 0.0$, the boundary becomes a zero-order extrapolation like the periodicity condition used in the original 2.5D approach.

A parametric study of the variation of this normal forcing factor in Fig. 10 with a constant extrusion length of 5 percent of the airfoil chord shows that as expected, the behavior of the aerodynamic coefficients follows the same trend when increasing the normal forcing factor as when reducing the extrusion length with the root symmetry condition in Fig. 9. Based on these results the new normal forcing boundary condition with an extrusion length of 5 percent of the chord is used to generate the viscous databases in the following results.

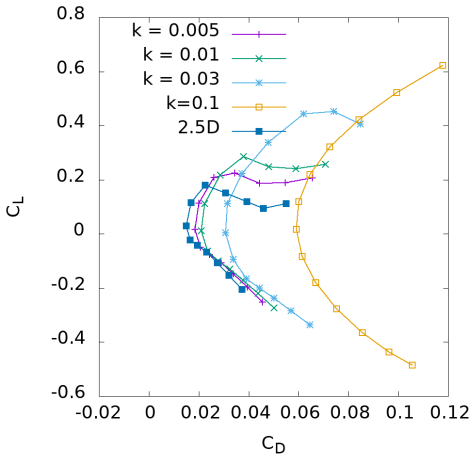

Figure 10: Parametric study of the k normal forcing factor when using the modified boundary condition for lift coefficient against drag coefficient and comparison with 2.5D approach (Ma=0.85, Re=8.46e6, $\phi_{c/4}$=31.4°)

4. NUMERICAL RESULTS ON WING-BODY CONFIGURATIONS

To analyze the effect of the new modifications on the complete NL-VLM solver, the NL-VLM with the modifications presented in Sec. 3 is used on wing-body configurations. The same test cases are also run with the NL-VLM implementation without the modifications to the viscous database for comparison. It should be noted that the modification to the inviscid slope used in the effective angle computation and presented in Sec. 3.1 is used in both cases. This allows the analysis to focus on the effect of the viscous database modification, the improvement in effective angle computation by the slope modification already having been showcased.

The first considered test case is case 1 of the first drag prediction workshop, which consists in enforcing a lift coefficient of 0.5 for the DLR-F4 wing-body geometry [9]. The flow conditions are a Reynolds number of 3 000 000 and a Mach number of 0.75, which are transonic conditions. For the NL-VLM computation, the viscous database is assembled from 4 RANS polars.

One is computed at the root of the wing, two are computed on each side of the kink of the wing to account for the sweep variation and one is computed for the tip airfoil section. For the new implementation, a normal forcing factor of 0.05 is used for the inboard normal forcing boundary condition in the root section database computation, based on a parametric study to identify an adequate value to avoid an increase of drag that would be too important. The wing surface solution is generated from the NL-VLM results through an interpolation of the surface solution of the RANS results used to assemble the database. The pressure coefficients of these reconstructed solutions are compared to the experimental pressure measurements from the ONERA wind tunnel for the first drag prediction workshop in Fig. 11 and Fig. 12. The sections considered are the two sections closest to the fuselage available.

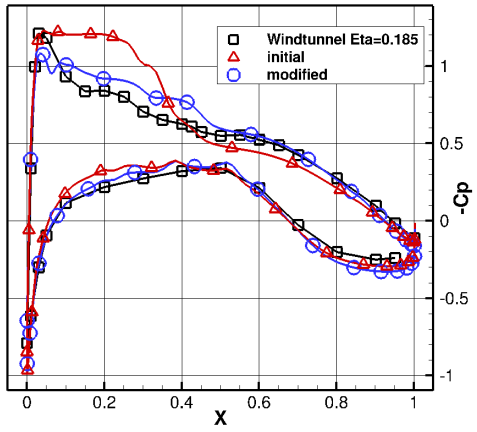

Figure 11: Comparison of the reconstructed solution of the initial NL-VLM and the modified implementation with experimental measurement as reference for the DLR-F4, section at 18.5% of the span

The results show that the new implementation avoids overpredicting a shock near the wing root. This overprediction of the shock by the unmodified method is consistent with results from a similar previous work [4]. Some discrepancies with experimental measurements are still present, notably in the second section measured along the span.

To analyze the effect of the modifications on the aerodynamic coefficients predicted by the NL-VLM, an angle of attack sweep is done on the DLR-F4 geometry in the same flow conditions and compared with experimental results from ONERA. For the drag computation, a constant value of 0.009 corresponding to wind tunnel measurements is added to the NL-VLM C_D result to model the fuselage drag since no viscous coupling is applied on the body. The results, in Fig. 13 and Fig. 14, show that while the modifications allow the method to predict a

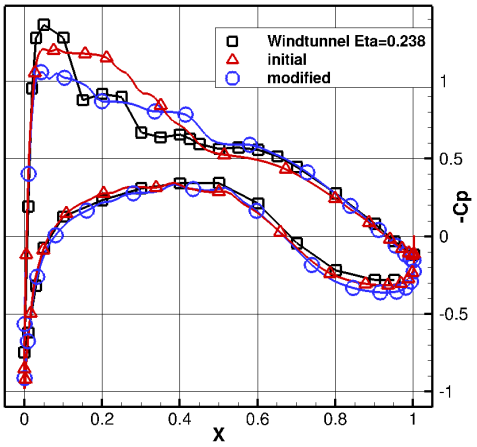

Figure 12: Comparison of the reconstructed solution of the initial NL-VLM and the modified implementation with experimental measurement as reference for the DLR-F4, section at 23.8% of the span

higher stall angle and maximum C_L which is closer to the experimental results, the drag seems to be overpredicted compared with experimental data. The drag predicted by the initial method is closer to the experimental results for lower angles of attack. As it was observed that the normal forcing modification to the viscous database caused an increase in the drag coefficient, these results seem to indicate that the overprediction of drag is a downside of this modification.

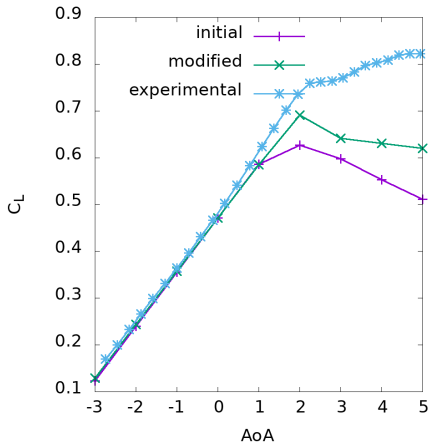

Figure 13: Lift coefficient against angle of attack of the original and modified NL-VLM implementation and experimental data for the DLR-F4 geometry in transonic conditions

A second test case is considered consisting of the high-speed Common Research Model wing-body geometry [18]. The first case of the fifth drag prediction workshop is used for the flow conditions, which are a lift coefficient enforced at 0.5, a Reynolds number of 5 000 000

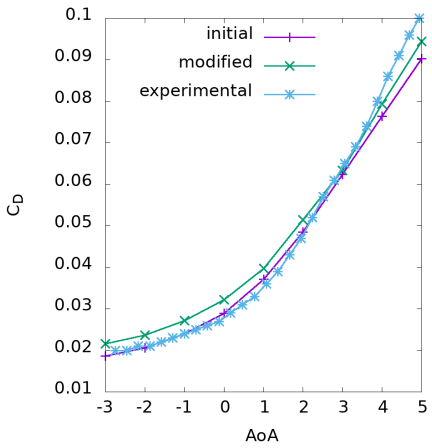

Figure 14: Drag coefficient against angle of attack of the original and modified NL-VLM implementation and experimental data for the DLR-F4 geometry in transonic conditions

and a Mach number of 0.85. The CRM wing shows significant airfoil variation along its span, and for this reason, in this case, 12 sections are considered to assemble the viscous database, distributed roughly at every 10% of the span from the root to the tip with the addition of the wing kink for which a section on either side is considered to take the sweep and taper change into account. Due to the instability in the nonlinear RANS solver caused by the tapered geometry modification to the database mentioned in Sec. 3.2, the tapered geometry modification is only applied to the first viscous section. The normal forcing factor used for the RANS boundary condition varies from 0.1 for the first section to 0.04 to the second and 0.01 for the third. The other sections are considered sufficiently far from the fuselage for this modification to be unnecessary.

The pressure coefficients over the reconstructed solution are again compared with experimental results from the National Transonic Facility for the same case for two sections near the fuselage in Fig. 15 and Fig. 16. It is again observed that while discrepancies are present between the NL-VLM and experimental results, the modified method is closer to the experimental pressure coefficients. In particular, the strong shocks predicted by the initial method near the wing root are not present in the modified method. The presence of these shocks in the original method is consistent with results from previous work on the same case, where it was reported that this wrong prediction near the wing root caused an early stalling of the inboard wing section [8].

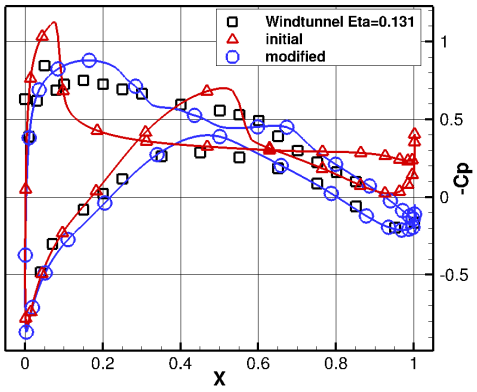

Figure 15: Comparison of the reconstructed solution of the initial NL-VLM and the modified implementation with experimental measurement as reference for the HS-CRM, section at 13.1% of the span

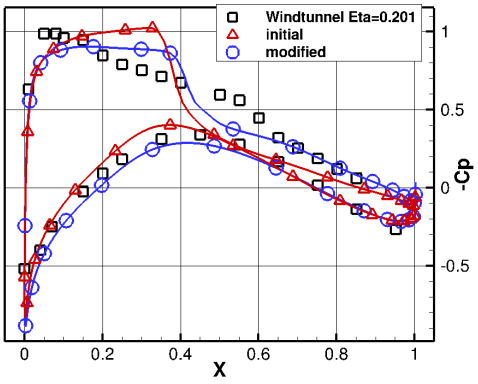

Figure 16: Comparison of the reconstructed solution of the initial NL-VLM and the modified implementation with experimental measurement as reference for the HS-CRM, section at 20.1% of the span

5. CONCLUSION

The aim of this paper was the exploration of methods to improve the prediction of shocks by the NL-VLM for transonic conditions in the region of the wing near the fuselage. To achieve this, three modifications to the original implementation were explored and integrated. The results obtained indicate that the modifications allow a more reliable prediction of flow physics. However, some discrepancies with experimental results remain and while the normal forcing correction seems to improve the shock prediction for sections near the fuselage, caution should be taken about the drag increase it causes.

6. ACKNOWLEDGEMENTS

This work benefits from FRQNT and NSERC doctoral scholarships as well as from the Canada Research Chair program.

REFERENCES

[1] J. Deyoung. Historical evolution of vortex-lattice methods. January 1976. NTRS Author Affiliations: Vought Corp. NTRS Document ID: 19760021076 NTRS Research Center: Legacy CDMS (CDMS).

[2] M. Drela. *Flight Vehicle Aerodynamics*. MIT Press, Cambridge, MA, USA, February 2014.

[3] M. Franciolini, A. Da Ronch, J. Drofelnik, D. Raveh, and A. Crivellini. Efficient infinite-swept wing solver for steady and unsteady compressible flows. *Aerospace Science and Technology*, 72:217–229, January 2018.

[4] S. Gallay and E. Laurendeau. Preliminary-Design Aerodynamic Model for Complex Configurations Using Lifting-Line Coupling Algorithm. *Journal of Aircraft*, 53(4):1145–1159, July 2016. Publisher: AIAA.

[5] S. Ghasemi, A. Mosahebi, and E. Laurendeau. A Two-Dimensional/Infinite Swept Wing Navier-Stokes Solver. In *52nd Aerospace Sciences Meeting*, AIAA SciTech Forum. AIAA, January 2014.

[6] J. Katz and A. Plotkin. *Low-Speed Aerodynamics*. Cambridge Aerospace Series. Cambridge University Press, Cambridge, 2 edition, 2001.

[7] A. Kontogiannis and E. Laurendeau. Adjoint State of Nonlinear Vortex-Lattice Method for Aerodynamic Design and Control. *AIAA Journal*, 59(4):1184–1195, 2021. Publisher: AIAA _eprint: https://doi.org/10.2514/1.J059796.

[8] A. Kontogiannis, M. Parenteau, and E. Laurendeau. Viscous-Inviscid Analysis of Transonic Swept Wings using 2.5D RANS and Parametric Shapes. In *AIAA Scitech 2019 Forum*, AIAA SciTech Forum. AIAA, January 2019.

[9] D. Levy, R. Wahls, T. Zickuhr, J. Vassberg, S. Agrawal, S. Pirzadeh, and M. Hemsch. Summary of data from the first AIAA CFD Drag Prediction Workshop. In *40th AIAA Aerospace Sciences Meeting & Exhibit*. AIAA, 2002.

[10] D. W. Levy, K. R. Laflin, E. N. Tinoco, J. C. Vassberg, M. Mani, B. Rider, C. L. Rumsey, R. A. Wahls, J. H. Morrison, O. P. Brodersen, S. Crippa, D. J. Mavriplis, and M. Murayama. Summary of Data from the Fifth Computational Fluid Dynamics Drag Prediction Workshop. *Journal of Aircraft*, 51(4):1194–1213, 2014. Publisher: AIAA.

[11] V. Liguori, F. Moens, J. Peter, and E. Laurendeau. Validation of a nonlinear Vortex Lattice Method for multiple wing sweep angle configurations. In *56th 3AF International Conference on Applied Aerodynamics*, March 2022.

[12] V. Liguori, F. Plante, and E. Laurendeau. Implementation of an efficient Selective Frequency Damping method in a RANS solver. In *AIAA Scitech 2021 Forum*, AIAA SciTech Forum. AIAA, January 2021.

[13] M. Parenteau, S. Bourgault-Cote, F. Plante, E. Kayraklioglu, and E. Laurendeau. Development of Parallel CFD Applications with the Chapel Programming Language. In *AIAA Scitech 2021 Forum*. AIAA, January 2021.

[14] M. Parenteau, K. Sermeus, and E. Laurendeau. VLM Coupled with 2.5D RANS Sectional Data for High-Lift Design. In *2018 AIAA Aerospace Sciences Meeting*, AIAA SciTech Forum. AIAA, January 2018.

[15] E Pistolesi. Considerations on the Mutual Interference of Aerofoil Systems. *L.G.L. Rep.*, pages 214–219, 1937.

[16] J. D. Taylor and D. F. Hunsaker. Low-fidelity method for rapid aerostructural optimisation and design-space exploration of planar wings. *The Aeronautical Journal*, 125(1289):1209–1230, July 2021. Publisher: Cambridge University Press.

[17] C.P. van Dam. On the aerodynamic design of multi-element high-lift systems. *Progress in Aerospace Sciences - PROG AEROSP SCI*, 38:101–144, February 2002.

[18] J. Vassberg, M. Dehaan, M. Rivers, and R. Wahls. Development of a Common Research Model for Applied CFD Validation Studies. In *26th AIAA Applied Aerodynamics Conference*, Guidance, Navigation, and Control and Co-located Conferences. AIAA, August 2008.

[19] Z.-M. Xu, Z.-H. Han, and W.-P. Song. An improved 2.75D method relating pressure distributions of 2D airfoils and 3D wings. *Aerospace Science and Technology*, 128:107789, September 2022.

[20] O. Şugar Gabor and A. Koreanschi. Fast and accurate quasi-3D aerodynamic methods for aircraft conceptual design studies. *The Aeronautical Journal*, 125(1286):593–617, April 2021. Publisher: Cambridge University Press.